RADIATION SHIELDING OF MAJOR PENETRATIONS IN TOKAMAK REACTORS

SHIELDING

KEYWORDS: *tokamak-type reactors, shielding, neutron reactions, geometry, Monte Carlo method, discrete ordinates method, buildings, radiations hazards*

JUNGCHUNG JUNG and MOHAMED A. ABDOU*
Argonne National Laboratory, Applied Physics Division
9700 South Cass Avenue, Argonne, Illinois 60439

Received March 22, 1978
Accepted for Publication June 23, 1978

The geometric representation and the multidimensional calculational method for neutronics analysis of tokamak reactors with major penetrations have been examined. It has been found that two-dimensional models are useful for scoping studies but that three-dimensional models are necessary for detailed design studies. The material and geometry requirements of local exterior penetration shields are examined. The level of radiation streaming is parametrized as a function of the penetration size and shape. A dual-purpose duct system in which the evacuation (vacuum pumping) ducts are connected to the neutral beam ducts at locations outside the bulk shield is an attractive approach. This system reduces the overall shield requirements and potentially permits orders of magnitude reduction in the radiation level at the vacuum pumps. A comparison of the two plasma supplementary heating methods—radio frequency (rf) and neutral beams—shows that the rf system offers considerable advantage over the neutral beam system in terms of lower shielding requirements and easier control of the radiation dose in the reactor building.

I. INTRODUCTION

The blanket/shield system in a tokamak reactor has to accommodate a variety of penetrations that serve various essential functions. Examples are penetrations required for (a) toroidal plasma chamber evacuation (vacuum pumping), (b) supplementary plasma heating, (c) impurity control (e.g., divertors), (d) access for diagnostics and maintenance, and (e) cooling. These various types of penetrations not only are different in their functional requirements but also have large differences in size, shape, and number. Recent studies[1-5] have shown that adequate shielding against radiation streaming from these penetrations is necessary for the successful operation of many reactor components. Furthermore, the studies of Refs. 1 and 2 have shown clearly that the interrelation between the penetration shields and the rest of the reactor is so strong that the shielding for penetrations must be considered at the early stages of the reactor design process.

There are two different approaches for shielding against radiation streaming. The first involves employing shield plugs that completely close the penetrations during the plasma burn. The second relies on surrounding the penetration as it emerges from the bulk shield with a local exterior shield that is shaped and positioned so as to provide adequate and effective shielding. It is not clear at present which approach should be utilized in tokamaks. The shield plug approach is useful only if the functional requirements of the penetration permit that it can be closed at all times that the fusion reaction rate is greater than zero. This excludes the shield plug for some penetrations such as that for a divertor. The situation is not as clear for other types of penetrations. For example, in all tokamaks, plasma supplementary heating is performed while the fusion reaction rate is appreciable, although not at full power. Therefore, if the shield plug is used in the plasma heating penetrations, it can be closed only during the peak portion of the plasma burn, and another method of shielding is required during startup. For penetrations that can employ either a shield plug or a local exterior penetration shield, the choice is also not clear. A shield plug has a relatively small impact on the reactor design but presents difficult automatic control and reliability problems.

*Present address: Georgia Institute of Technology, School of Nuclear Engineering, Atlanta, Georgia 30332.

A local exterior penetration shield, on the other hand, has a relatively large impact on the reactor design. Such an impact is exemplified by the substantial modifications in the reactor geometry needed to accommodate the local exterior penetration shields.

Resolving these questions will require more detailed comparative engineering, safety, and economics studies. These studies require an extensive quantitative information base in several technical areas. The work reported in this paper seeks to develop such information for the neutronics area. The neutronics analysis of the shield plug is straightforward and is not treated here. The focus of this work is on the more involved problems of the local exterior penetration shields. Moreover, the scope of the work is limited to the major penetrations of vacuum pumping and plasma supplementary heating.

The remainder of this paper is organized as follows. The computational methods and the geometric representation are discussed in Sec. II. The sensitivity of radiation streaming to the neutral beam duct size and shape is investigated in Secs. III and IV. In Sec. V we examine a dual-purpose duct system in which the toroidal chamber evacuation system shares with the auxiliary heating system the same ducts that have to penetrate the blanket and bulk shield. Radio frequency (rf) heating represents an attractive alternative to neutral beam heating. From a shielding point of view, rf heating has a distinct advantage in that bends can be introduced into the waveguide ducts in sharp contrast to neutral beams, which require a straight-through path from the first wall to the beam injector located outside the toroidal field (TF) coils. A representative rf system is examined and compared to a neutral beam system in Sec. VI. Section VII is devoted to an analysis of neutron spectra along the radiation streaming path through penetrations.

II. COMPUTATIONAL METHODS

Three areas of prime concern in treatment of penetrations are

1. geometric representation of the reactor system
2. selection of a solution method for predicting the neutron and photon transport
3. selection of approximations and special techniques to reduce the computational time for a desired accuracy.

The special characteristics of tokamaks make the process of selecting a computational approach troublesome.

A basic feature of a tokamak is the toroidal geometry. Recent work[1,2] has shown that an explicit treatment of toroidal geometry is not necessary for penetration scoping studies. Nevertheless, accounting for the other details in the reactor configuration still requires a three-dimensional geometrical representation. The degree of detail in such a three-dimensional geometrical representation will greatly affect the computational time. Therefore, omitting the nonessential details is very desirable for scoping studies. An example is a three-dimensional geometrical model that was developed in Ref. 1 for treatment of major penetrations and that is illustrated in Fig. 1. The figure is a schematic diagram of a cross section in a z-x plane formed by the toroidal magnetic axis (a straight line when toroidal curvature is ignored) and the axis of a vacuum duct. A view in the x-y plane (see the figure) shows a cross section of the

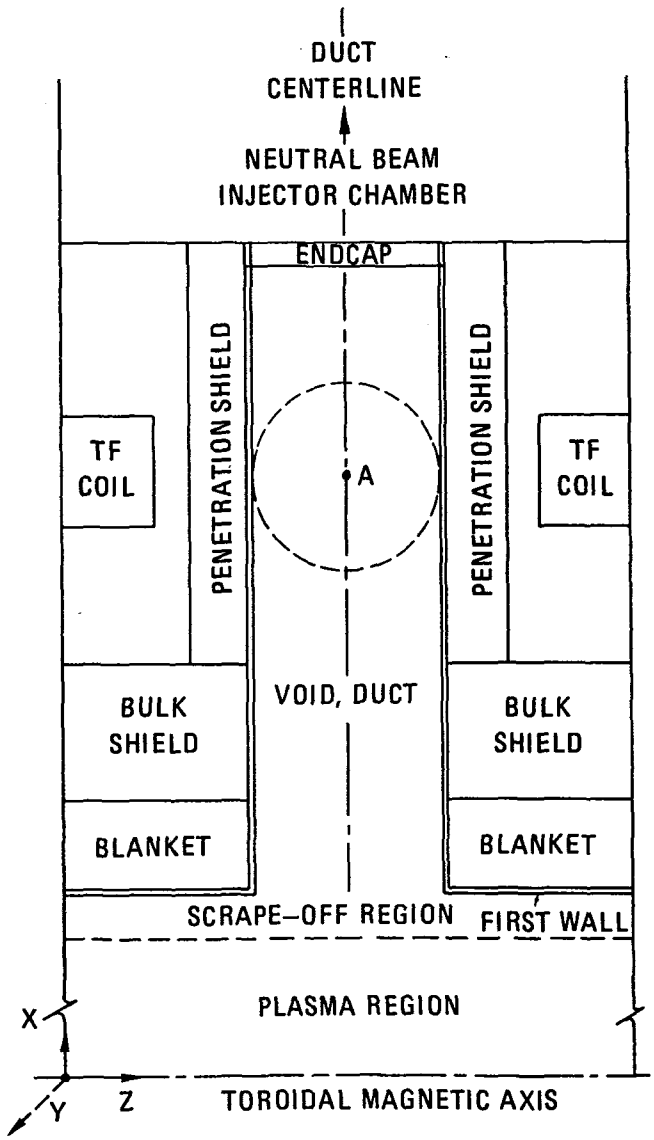

Fig. 1. A schematic diagram of a typical neutral beam system showing a local exterior penetration shield.

plasma (circular, D-shaped, or doublet) and the TF coils (e.g., constant-tension D shape), with the first wall, blanket, and bulk shield regions forming sets of concentric regions surrounding the plasma. A tokamak has a number of TF coils that are located equally spaced around the torus. Only one segment of the reactor that extends between the symmetry vertical planes for two neighboring TF coils needs to be treated.

Two transport methods can be considered for analysis of penetrations: Monte Carlo and discrete-ordinates, S_N. The S_N method has the tremendous advantage of providing a deterministic solution everywhere in the entire system. Unfortunately, attempts to utilize the S_N method for three-dimensional problems have not been successful, and at present the method is considered impractical for three-dimensional calculations. The Monte Carlo method, on the other hand, is a very powerful tool, particularly for complicated geometries. However, this method is inherently machine- and man-time consuming for the shielding problems considered here, primarily for two reasons:

1. deep radiation penetration (five to eight orders of magnitude radiation attenuation is typical)
2. the need for a detailed transport solution almost everywhere in the reactor system.

The work of Ref. 1 examined this problem using the continuous energy Monte Carlo code VIM (Refs. 6 and 7), and a sample of the results is reproduced in Table I. The geometry analyzed is similar to that of Fig. 1, and two cases are shown, one with a duct diameter of 0.2 m and another with an 0.85-m-diam duct. The 0.2-m duct case has no provision for a special penetration shield, but the 0.85-m duct is surrounded as it emerges from the bulk shield with a local exterior penetration shield that almost fills the space between the TF coils. The number of source neutron histories is 50 000 for the small duct and 30 000 for the larger duct. One can observe from Table I the poor statistics of the solution (the standard deviation is shown in parenthesis) at the endcap region (see Fig. 1) and the TF coils for the small duct case. Better statistics are obtained for the larger duct case in regions inside and in the immediate vicinity of the penetration because of the enhanced radiation streaming for such a large duct. However, the statistics are poor at the TF coils because of the presence of a local penetration shield. It should be noted that to eliminate the penetration effects, the local penetration shield must be improved to provide several orders of magnitude of radiation attenuation. This will reduce the probability of a neutron reaching the TF coils and in turn will require a dramatic increase in the number of source neutron histories required for a reasonable accuracy. It should be noted that many splitting surfaces were used to calculate the results in Table I, but the use of additional variance reduction techniques could probably improve the accuracy of the solution. Two conclusions can be made from the results in Table I. Smaller size

TABLE I

Comparison of Results Obtained with Three-Dimensional Monte Carlo for Small- and Large-Size Penetrations

Thickness of bulk shield, m	1.31	1.31
Diameter of penetration duct, m	0.20	0.85
Penetration shield composition	---	50% stainless steel + 50% B_4C
Dimensions of penetration shield	---	t_1 = 0.75 m[a] t_2 = 0.34 m l_1 = 0.59 m l_2 = 0.15 m
Number of histories	50 000	30 000
Flux[b] (n/m²·s)		
at duct wall inside bulk shield	8.65(17) (±7%)	1.41(17) (±3%)
at duct wall outside bulk shield	5.16(15) (±64%)	2.36(15) (±5%)
at endcap	5.35(15) (±100%)	1.28(17) (±7%)
at TF coil	1.10(14) (±56%)	1.32(13) (±79%)
Leakage/DT neutron	8.26(−5) (±45%)	8.80(−3) (±5%)

[a] t_1 = penetration shield thickness in the region between the bulk shield and inner surface of the TF coils

t_2 = penetration shield thickness in the region between the TF coils

l_1 = penetration shield length in the region between the bulk shield and inner surface of the TF coils

l_2 = penetration shield length in the region between the TF coils.

[b] Normalized to a neutron wall load of 1 MW/m².

ducts are more computer-time consuming than larger ducts. In addition, as the shield effectiveness is improved, the computational difficulties increase substantially. It should be emphasized that the purpose of this paper is to scope and identify the problems associated with penetration shielding in tokamaks. Future studies are needed to investigate means of improving the accuracy and reducing the computational time in the specialized geometries of tokamaks, particularly with small-size penetrations.

Much of the results to be reported in the following sections were obtained using a three-dimensional geometrical model with the Monte Carlo code VIM. However, the difficulties discussed above provided a strong motive toward seeking the possibility of two-dimensional geometrical models that can be used in the early stages of scoping design studies. One of these that is utilized extensively in this work is described below. This two-dimensional model focuses on penetrations, penetration shields, and other regions most affected by radiation-assisted streaming. This model offers a substantial computational time cost saving compared with the more elaborate three-dimensional models. More important, it makes it possible to employ the S_N method to obtain a solution everywhere in the vicinity of penetrations. This is required at some stages of the design process, but it proved cost prohibitive with three-dimensional Monte Carlo calculations.

The geometric model consists basically of a set of concentric cylinders with the penetration axis as the common axis. In (r,z) coordinates, the origin is at the plasma geometric center, and the z axis is taken along the common axis. The basic approximation comes from assuming that the outer surface of the shield is cylindrical. Therefore, one does not expect the model to be accurate near the boundary. However, the solution to the neutron transport equation is found to be reasonably accurate in the regions inside and in the vicinity of the penetration. This is due to the fact that the neutron behavior in these regions is governed primarily by neutron streaming rather than by neutron transport from regions near the boundary. We discuss this point in more detail shortly.

The sensitivity of the results obtained with this two-dimensional model to the order of S_N and P_L approximations is examined here for two typical types of penetrations. Type A is a large-size penetration with 0.85 m as the diameter of the duct. Type B is a small-size penetration 0.2 m in diameter. A blanket/bulk shield system of stainless steel and boron carbide ~1 m thick was employed. A local exterior penetration shield 0.5 m thick for Type A and 0.2 m thick for Type B was also incorporated into the calculation. A neutron energy group structure that extends from 14.1 to ~5 MeV was utilized in the S_N-P_L convergence tests to save on computational time. Monte Carlo calculations were also performed using VIM for both Types A and B to provide a base for testing the convergence.

For Type A, Table II shows the neutron fluxes at several key locations with various S_N-P_L approximations. The S_8-P_3 agrees with the S_{12}-P_3 within ~20% in the penetration shield region. The S_{12}-P_3 solutions converge to those of VIM within the statistical variance except for region 1. In region 1, all the S_N approximations examined yield the converged solution, and the standard deviation with VIM is very small. A possible source of the discrepancy between the two solutions of VIM and S_N in region 1

TABLE II

Convergence of S_N-P_L Approximation with the Two-Dimensional Model

Type A: Duct Diameter = 0.85 m, Penetration Shield Thickness = 0.5 m

Region	Flux ($E \geq 5.5$ MeV)/DT Neutron (n/m^2·s)			
	S_6-P_3	S_8-P_3	S_{12}-P_3	VIM (40 000)
1. Blanket/shield region (0 to 0.3 m from duct and 0 to 0.1 m from first wall)	1.16(−1)	1.15(−1)	1.15(−1)	1.28(−1) (±0.4%)
2. Penetration shield region (0 to 0.3 m from duct and 1.2 to 1.5 m from end of bulk shield)	4.59(−4)	3.55(−4)	2.94(−4)	3.17(−4) (±22%)
3. TF coil region (0.1 to 0.2 m from magnet inner surface)	3.34(−7)	3.39(−7)	3.56(−7)	2.76(−7) (±28%)

TABLE III

Convergence of S_N-P_L Approximation with the Two-Dimensional Model

Type B: Duct Diameter = 0.2 m, Penetration Shield Thickness = 0.2 m

Region	Flux ($E \geq 5.5$ MeV)/DT Neutron (n/m^2·s)			
	S_6-P_1	S_8-P_3	S_{12}-P_3	VIM (27 000)
1. Blanket/shield region (0 to 0.2 m from duct and 0 to 0.25 m from first wall)	5.31(-2)	5.45(-2)	5.45(-2)	6.14(-2) (±3%)
2. Penetration shield region (0 to 0.2 m from duct and 1.0 to 1.15 m from end of bulk shield)	3.41(-9)	3.69(-8)	1.92(-7)	2.33(-7) (±94%)
3. TF coil region (0 to 0.15 m from magnet inner surface)	1.22(-9)	5.29(-9)	1.07(-8)	4.4(-9) (±43%)

may, therefore, be attributable to the fact that an ENDF/B-III library[8] was used for the S_N calculations, while the VIM calculation was done with the ENDF/B-IV version.[9] This will be clarified later.

Neutron fluxes with various S_N-P_L approximations for the smaller size (Type B) penetrations are shown in Table III. Convergence is difficult here, and the S_8-P_3 result can be a factor of 5 to 6 lower than the S_{12}-P_3 solution in the local shield region. For these small ducts, it is also difficult to obtain a good accuracy with Monte Carlo in many regions of the problem if only a moderate number of neutron histories are tracked.

As mentioned earlier, the transport calculation for small-size penetrations is an area where future research is required to investigate methods for improving accuracy. For example, exploring different variance reduction techniques in Monte Carlo and biased angular quadrature sets for the S_n calculations will be useful.

The validity of the two-dimensional model and its applicability to penetration shielding analysis was made by comparing the results obtained with the model to those from Monte Carlo calculations for the three-dimensional system that the two-dimensional geometry is intended to approximate. The dimensions and material compositions employed for the analysis are summarized in Table IV along with the neutron fluxes at several locations of interest. The Monte Carlo calculation was carried out with ENDF/B-IV data using 30 000 source neutron histories. The neutron energy is treated continuously from 14.1 MeV down to the thermal energy. The neutron transport equation in the two-dimensional model was solved with the S_6-P_3 approximation using a 20-energy-group structure.

TABLE IV

Validation of the Two-Dimensional S_N Calculations

Thickness of bulk shield, m	1.31	
Diameter of penetration duct, m	0.85	
Penetration shield composition	50% stainless steel + 50% B_4C	
Dimensions of penetration shield	$t_1 = t_2 = 0.3$ m[a] $l_1 + l_2 = 1.19$ m	
Flux[b] (n/m^2·s)	VIM/30 000	S_6-P_3
1. Duct wall inside bulk shield	1.53(18) (±3%)	1.59(18)
2. Duct wall outside bulk shield	2.88(17) (±5%)	3.36(17)
3. Endcap	1.67(17) (±7%)	2.30(17)
4. TF coil	9.69(14) (±20%)	3.45(15)
5. Leakage/DT neutron	4.04(-3) (±7%)	5.42(-3)

[a] t_1 = penetration shield thickness in the region between the bulk shield and inner surface of the TF coils

t_2 = penetration shield thickness in the region between the TF coils

l_1 = penetration shield length in the region between the bulk shield and inner surface of the TF coils

l_2 = penetration shield length in the region between the TF coils.

[b] Normalized to a neutron wall load of 1 MW/m^2.

A multigroup cross-section set was collapsed from the DLC-37 library[10] generated from ENDF/B-IV with the AMPX system.[11] The results in Table IV obtained by both the Monte Carlo and S_N methods are based on the same basic nuclear data, ENDF/B-IV. It is seen from these results that the two-dimensional model can actually reproduce the three-dimensional results to better than 30% accuracy except in the TF coils. The two-dimensional model overestimates the neutron flux in the TF coil by a factor of ~4. The reason for this is that

the geometrical representation of the TF coils in the two-dimensional geometrical model is the most approximate of all regions. With reference to Fig. 1, the actual (three-dimensional) geometry of the TF coil is such that they rotate around the x axis (viewed in the x-y plane, they show a D or circular shape), but in the two-dimensional geometrical model they rotate around the axis of the duct, which is parallel to the x axis (viewed in the z-y plane, they show a circular shape). This geometrical approximation in the two-dimensional model makes a larger volume of the TF coils close to the penetration duct. Nevertheless, even for the TF coils, the two-dimensional model is valuable for comparative and scoping studies on penetrations, since this two-dimensional model requires much less computational time than the three-dimensional calculations. It should be noted that when the same nuclear data are used in both the Monte Carlo and S_N calculations, excellent agreement is obtained on the neutron fluxes in the blanket and bulk shield regions, as shown in Table IV. This provides the basis for our earlier assumption that the difference in the result of the two methods given in Tables II and III is attributable to the difference in nuclear data.

III. EFFECTS OF DUCT SIZE

The initial phases of a reactor design process involve an investigation of many types of trade-offs aimed at identifying the most promising options for a better performance and lower cost of the reactor. Our work included developing an information base on the nuclear effects of penetrations. In this section, we examine these effects as a function of the duct size for neutral beams. It should be noted that the ducts are essentially vacuum ducts and, hence, the results are applicable in many respects for similar ducts that serve other functions.

A simplified reference two-dimensional model similar to that described in the previous subsection with a 1-m-thick blanket/bulk shield was chosen for the scoping study presented in this section. The dimensions and the material compositions are given in Table V. The selection of a 1-m-thick bulk shield is based on the observation that the primary radiation streaming effect is somewhat insensitive to the thickness of the bulk shield. According to Ref. 1, increasing the bulk thickness of the blanket/shield from 0.9 to 1.3 m reduces the neutron flux at the TF coils by only a factor of ~3 when major penetrations are present. The penetration sizes considered in the present analysis cover the range d = 0.2 to 1.0 m and l = 2 to 5 m, where d is the duct opening diameter at the first wall and l is the duct length from the first wall to the front surface of the beam injectors. The material composition of the penetration shield is 50% stainless steel + 50% B_4C in all cases. The selection of this composition is also based on the results of Ref. 1, in which it is shown that the 50% stainless-steel + 50% B_4C penetration shield is a very effective attenuator at a reasonable cost.

TABLE V

Dimensions and Material Compositions of the Blanket and the Bulk Shield

	Radius, r (m)
Plasma	0-1.00
Vacuum	1.00-1.05
Stainless-steel first wall/blanket	1.05-1.35
50% stainless-steel + 50% B_4C bulk shield	1.35-2.05
Vacuum	2.05-4.20
Superconducting TF coils	4.20-5.10

In the following, some of the scoping study results for the nuclear effects of the neutral beam ducts are presented. These effects are examined in four regions:

1. components located inside the beam injector
2. superconducting TF coils
3. bulk shield regions in the vicinity of the beam ducts
4. coils located in the blanket region such as the F coils in a doublet,[12] or equilibrium coils, or initiation-trimming coils that may be present.

The computations were carried out with S_{12} for d = 0.2 m, S_8 for d = 0.4 to 0.6 m, and S_6 for d = 0.8 to 1.0 m. In all cases, the angular distributions of neutrons and photons were considered in the P_3 approximation.

III.A. Beam Injector

Figure 2 shows the maximum nuclear heating in the walls of the beam injectors as a function of duct diameter, d, at several values of the duct length, l. These results show that radiation streaming to the beam injector is a strong function of the penetration size. For small penetrations ($d < 0.4$ m), the heating rate varies much more strongly with both length and diameter of the duct than it does for larger size penetrations ($d > 0.6$ m). For example, the heating in the walls of the injector is reduced by only an order of magnitude when l is increased from 2 to 5 m for $d \approx 1$ m, while a difference of 1 m in duct length results in reduction in the injector heating of a factor of ~10 for $d \approx 0.2$ m.

It should be recalled from the results in the previous section, however, that convergence of the S_N results is very difficult for small-size penetrations

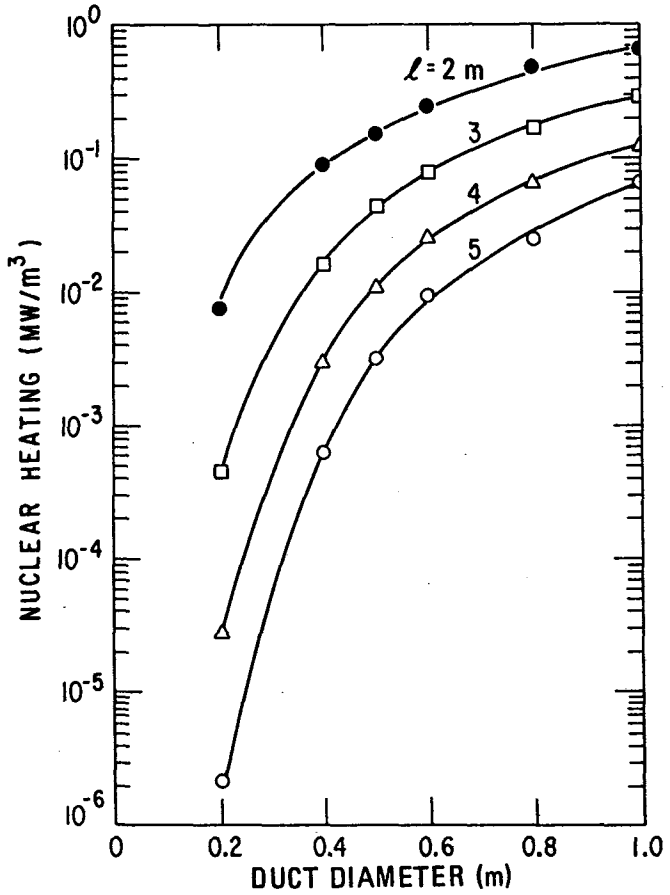

Fig. 2. Maximum nuclear heating in the beam injector wall as a function of duct diameter for several values of the duct length, l. (Neutron wall load is 1 MW/m^2.)

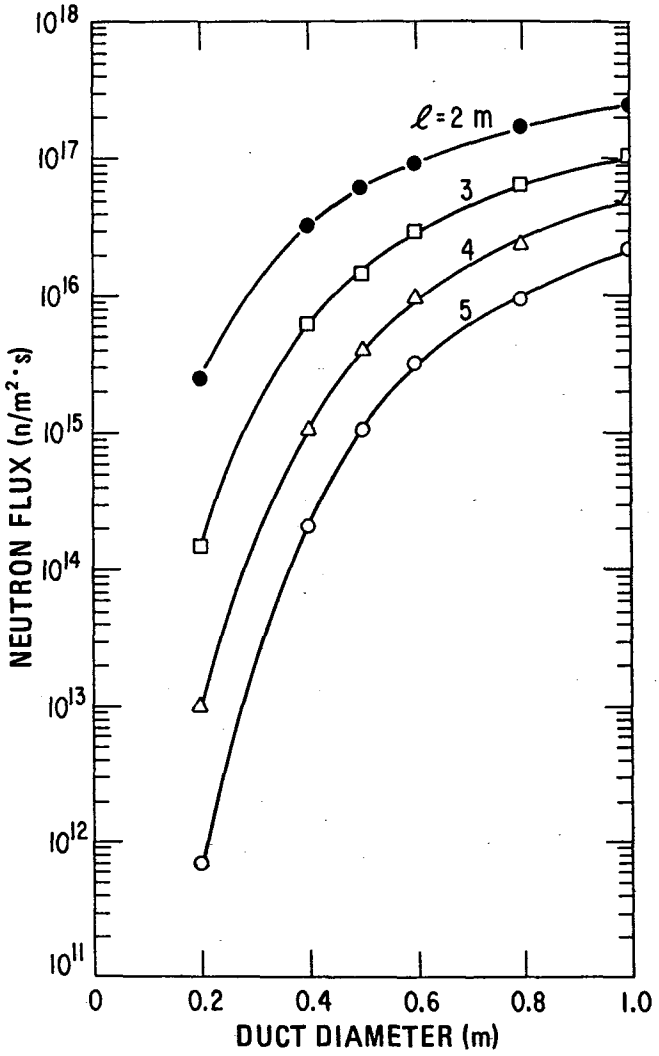

Fig. 3. Maximum neutron flux in the beam injector wall as a function of duct diameter for several values of the duct length, l. (Neutron wall is 1 MW/m^2.)

(~0.2 m or less). Therefore, it is likely that the S_{12} approximation employed here overestimates the neutron attenuation along the duct.

The vacuum pumping panels in the beam injector will be located at the immediate interior of the injector walls. If the material composition of the cryopanels is substituted by stainless steel, then the heating in the pumping panels is similar to that shown in Fig. 2. Acceptable radiation limits in cryopanels need to be defined in future experimental work. A preliminary analysis indicates that the nuclear heating probably needs to be limited to ~0.01 MW/m^3 to provide for a practical low-temperature cooling capability. Figure 2 shows that for a beam duct that is 4 m long, cryopanels can be used only if the beam duct diameter is <0.5 m if the nuclear heating is to be limited to 0.01 MW/m^3. Zirconium-aluminum vacuum pumping panels[12] can be successfully operated for the lifetime of the machine with duct sizes as large as 1 m in diameter. Figure 3 shows the maximum neutron flux in the beam injector as a function of d and l. The results in Fig. 3 exhibit the same functional dependence as those in Fig. 2.

III.B. TF Coils

The components of the superconducting TF coils must be adequately protected from radiation. One of the primary functions of the penetration shields is to reduce the nuclear radiation in the TF coils to the levels tolerated in the complete absence of penetrations. The tolerable nuclear radiation levels in the TF coils[2,13] have to be established in terms of the maximum allowable characteristic change or degradation of the components of the superconducting magnets such as (a) resistivity increase in the copper stabilizer, (b) decrease of critical current density in the NbTi superconductors, and (c) deterioration in the mechanical and dielectric properties of the electrical and thermal insulation.

Some results of the radiation damage relevant to the TF coil characteristics are discussed. Figures 4

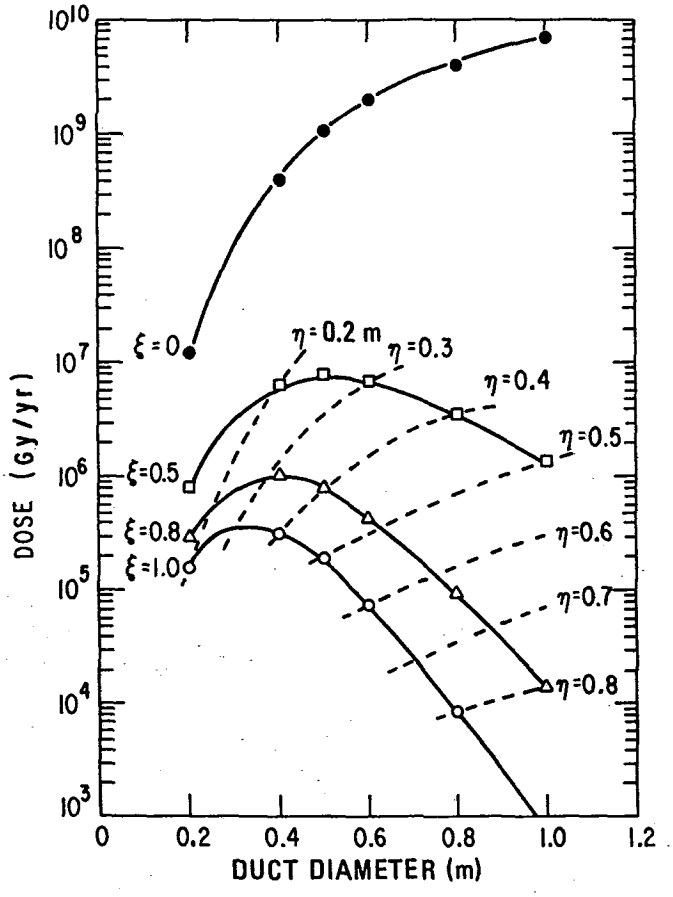

Fig. 4. Maximum nuclear dose in epoxy insulator of the TF coil as a function of duct diameter and penetration shield thickness for a neutron wall load of 1 MW/m².

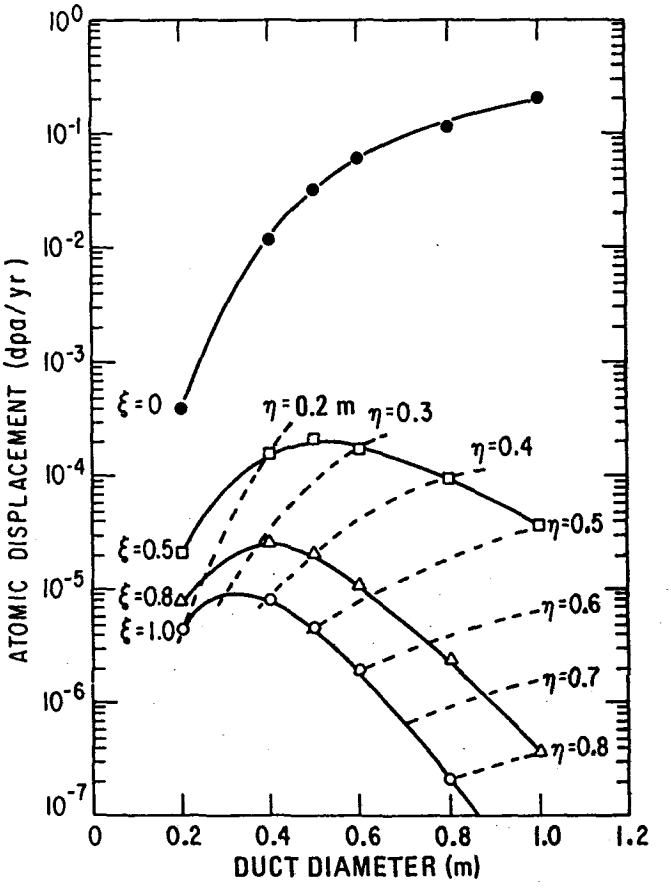

Fig. 5. Maximum atomic displacement in copper stabilizer of the TF coils as a function of duct diameter and penetration shield thickness for a neutron wall load of 1 MW/m².

and 5 show the dose in epoxy-base insulators and the atomic displacements in the copper stabilizer, respectively, as a function of the beam duct diameter and the thickness, η, of the local exterior beam duct shield. In these figures, the parameter ξ is defined as the ratio of the beam duct shield thickness to the beam duct diameter, i.e., $\xi = \eta/d$. The radiation levels in these two figures are those for an integral neutron wall loading of 1 MW·yr/m², where the integral neutron wall loading is the product of the neutron wall load, the operation time, and the plant duty factor. The figures can be used, however, to derive results at any integral neutron wall loading, since the radiation level varies linearly with this quantity. The radiation dose limit[14] to the epoxy insulator is ~10^7 Gy. The radiation damage to organic insulators is irreversible and, therefore, these insulators have to function properly for the lifetime of the reactor, which is ~30 yr for a commercial power plant. From Fig. 4, it is seen that for a 0.6-m-diam beam duct, the shielding ratio ξ varies from ~0.5 to ~0.7 as the neutron wall loading is increased from 0.1 to 10 MW/m². Radiation damage to the copper stabilizer and NbTi superconductor can be recovered by warming up the magnet. Therefore, the tolerable radiation dose to copper and NbTi must evolve from a trade-off study for the entire reactor.[13]

It is noted from Figs. 4 and 5 that for a fixed ξ, the radiation level at the TF coils increases as the beam duct diameter is increased until it reaches a maximum at $d \approx 0.4$ m; it then decreases again for larger size ducts. However, the required penetration shield thickness always increases as d increases. This can be seen by examining the η lines at a fixed dose in two figures.

III. C. Bulk Shields

Some results of the scoping study on the nuclear streaming effects on the duct wall surface are given in Figs. 6 and 7. The results are shown for several duct diameters. All figures are those along the wall of the duct as a function of distance apart from the plasma chamber. Figure 6 shows the neutron flux at

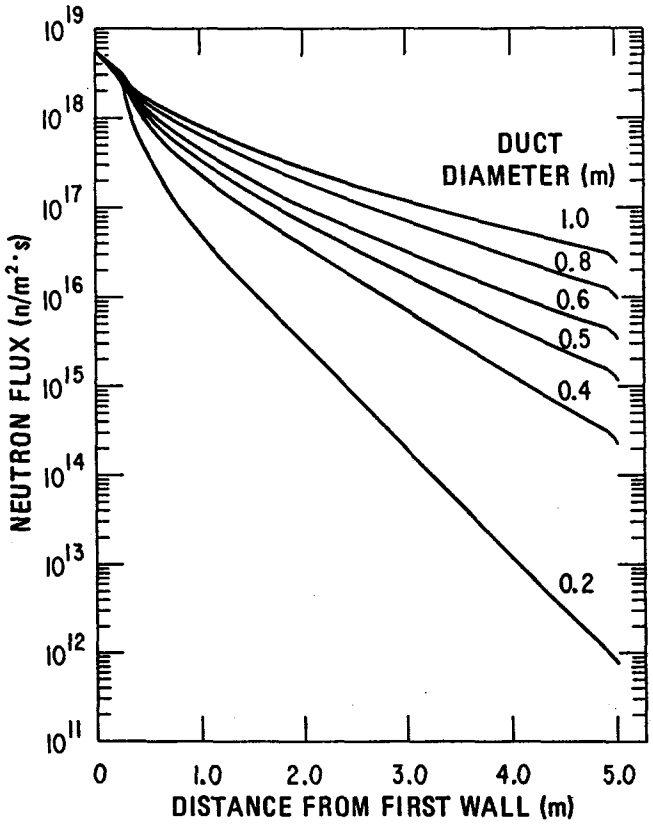

Fig. 6. Neutron flux along duct wall for various duct diameters as a function of distance from the first wall for a neutron wall load of 1 MW/m².

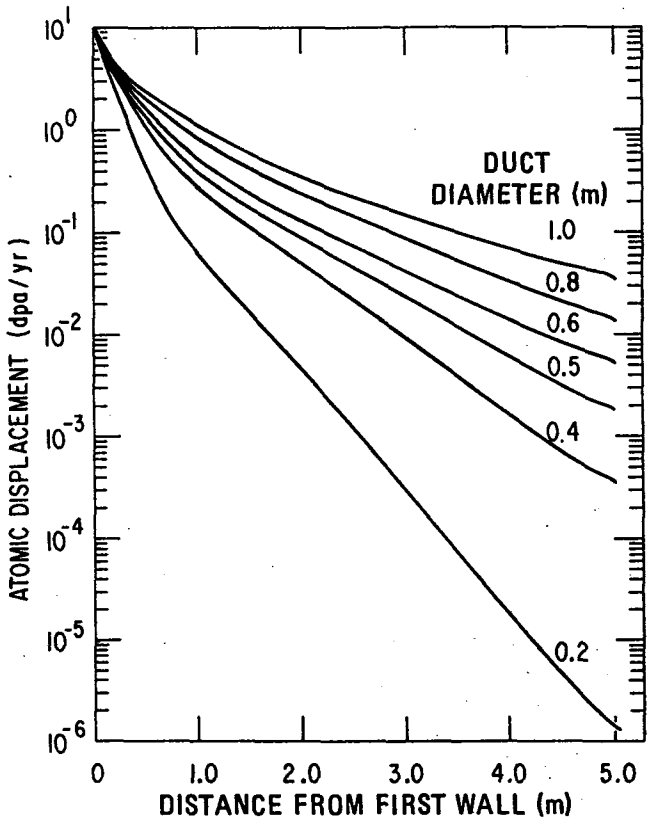

Fig. 7. Atomic displacement along duct wall for various duct diameters as a function of distance from the first wall for a neutron wall load of 1 MW/m².

a neutron wall loading of 1 MW/m². In Fig. 7, the atomic displacement in stainless steel is given for a neutron wall loading of 1 MW/m². An important observation to be made from these results is that the variation of nuclear radiation along the duct wall is very small compared to the radial attenuation in the bulk shield far away from the penetrations. For example, the flux attenuation along the duct between the first wall and the end of the bulk shield (~1 m long) is only a factor of 10 for $d > 0.4$ m. Usually in the same distance, we have a flux attenuation of about six orders of magnitude in regions far removed from the duct. This implies that in the neighborhood of the duct wall, special considerations similar to those of the first wall/blanket must be taken in all relevant technical areas such as thermal hydraulics, material selection, and mechanical engineering.

III.D. Coils Located in the Blanket

Table VI presents the dependence of the maximum neutron fluence and dose in inorganic insulators of coils located in the blanket (F coils) on the duct size for an integral neutron wall load of 1.0 MW·yr/m². No provision for shielding was made between the first wall and the F coils in this calculation. Apparently, the response rates are almost saturated to those at the first wall. The overall high neutron fluence and irradiation level reveal that the protection of the F coils is one of the critical issues to be solved in this type of reactor where the field-shaping coils or any other type of coils are located in a very high nuclear radiation field. It is obvious that organic insulators, such as Mylar and epoxy resin, cannot be used as the F coil insulators. If the maximum allowable dose in the Al_2O_3 insulator is ~10^{10} Gy (Ref. 15), then the insulators in an F coil located

TABLE VI

Maximum Neutron Fluence and Dose in F Coil Insulator (Al_2O_3) Versus Duct Diameter, d, for an Integral Wall Loading of 1 MW·yr/m² with No Shielding Between the First Wall and the F Coil

	d = 1 m	d = 0.5 m	d = 0.2 m
Neutron fluence, n/m²	1.6(26)	1.6(26)	1.6(26)
Dose, Gy	7.0(10)	6.7(10)	6.3(10)

immediately behind the first wall would operate successfully only up to an integral neutron wall load of ~0.1 MW·yr/m^2.

Table VII shows how the insulator lifetime can be prolonged by an additional shield for the F coil protection. For example, with an integral wall loading of 1 MW·yr/m^2, the dose at the F coil could be limited to 1.4×10^{10} Gy if the F coils were separated from the first wall and the beam duct wall by 0.15 m of shielding on both sides. The F coils have to be located much farther away from the first wall if operation to higher integral neutron wall loads is desired as in the case in commercial devices.

IV. EFFECTS OF DUCT SHAPE

In the previous section, we examined the sensitivity of radiation streaming to the duct size. In this section, the effects of the duct shape are investigated for a limited number of cases.

Calculations were made using the continuous energy Monte Carlo code VIM with 20 000 source neutron histories for several shapes of the duct cross section:

1. circle
2. square
3. elongated rectangle (elongated in the direction (z axis in Fig. 1) parallel to the toroidal magnetic axis
4. rectangle that is elongated in the direction (y axis in Fig. 1) perpendicular to the midplane (x-z plane in Fig. 1) of the torus.

Table VIII summarizes the results of the analysis. Specifications of the bulk shield and penetration shield material compositions and dimensions are also shown in Table VIII. In cases 1 through 4, the cross-sectional area of the duct was held constant and equal to ~0.567 m^2. The neutron flux in item a of Table VIII is the average neutron flux over the portion of the duct wall embedded in the blanket/bulk shield. The neutron flux in item b is the average over the portion of the duct wall external to the blanket and bulk shield. Table VIII shows that there is little variation in the neutron flux (a and b), but there is a small decrease as the duct shape is changed from a circle to a square and to a rectangle, i.e., the flux is lower for ducts with larger perimeter volumes. Note that the duct size examined here is relatively large. It is likely that a stronger dependence of radiation streaming on the duct shape exists for smaller size ducts.

The maximum neutron flux in the beam injector is 1.7×10^{17} n/m^2·s at a neutron wall load of 1 MW/m^2 for the circular duct. This flux is ~2% lower for the square duct and is ~25% lower for the rectangular duct.

It is found that the maximum radiation level at the TF coils is remarkably enhanced in case 3, in which the duct is elongated in the direction parallel to the toroidal magnetic axis, namely, the duct opening is located most closely to the magnets.

TABLE VII

Maximum Dose in F Coil Insulator (Al_2O_3) Versus Shield Thickness*

t_1 (m)	t_2 (m)			
	0	0.05	0.10	0.15
	[Dose (Gy/MW·yr/m^2) X 10^{-10}]			
0	6.7	4.9	3.8	3.0
0.05	6.2	4.0	2.7	1.9
0.10	6.1	3.7	2.3	1.5
0.15	6.1	3.6	2.1	1.4

*t_1 = shield thickness between duct and F coil
t_2 = shield thickness between first wall and F coil.

V. A DUAL-PURPOSE DUCT SYSTEM

It is clear from the results in the previous sections that the major penetrations have a substantial impact on a tokamak reactor design. A substantial fraction of the effective space of the blanket/bulk shield is occupied by penetrations that cause a significant loss in useful energy recovery and tritium breeding in future reactors. Furthermore, providing local exterior shields for penetrations that have to pass in locations with small spacing between the TF coils is a challenging problem. Therefore, it is important that every effort be pursued to minimize the number and size of ducts that have to penetrate the blanket and bulk shield. This provides a strong motive to examine a dual-purpose duct system for supplementary plasma heating and toroidal chamber evaluations, as illustrated schematically in Fig. 8 for an experimental power reactor.[16]

In this concept, the torus evacuation ducts are connected to the neutral beam or rf ducts at locations outside the blanket/bulk shield. This eliminates the need for separate evacuation ducts that penetrate the blanket/bulk shield with direct streaming of the plasma neutrons. The connected duct system has several advantages over the separate duct system. These include

1. a reduction in total radiation streaming through the combined duct system
2. substantial reduction in the fraction of the blanket volume occupied by penetrations.

TABLE VIII

Effect of Duct Opening Shapes

Case[a]	1	2	3	4
Opening Area	$\pi d^2/4$ d = 0.85 m	a^2 a = 0.753 m	$a_y \times a_z^b$ a_z = 0.940 m a_y = 0.604 m	$a_y \times a_z^b$ a_z = 0.604 m a_y = 0.940 m
	Neutron Flux[c] (n/m^2·s)			
a. Duct wall inside blanket/bulk shield	1.45(18) (±5%)	1.40(18) (±3%)	1.33(18) (±3%)	1.34(18) (±4%)
b. Duct wall outside blanket/bulk shield	2.80(17) (±6%)	2.46(17) (±4%)	2.25(17) (±5%)	2.25(17) (±7%)
c. Beam injector (maximum)	1.71(17) (±10%)	1.67(17) (±6%)	1.29(17) (±9%)	1.31(17) (±12%)
d. TF coil (maximum)	7.06(14) (±21%)	6.00(14) (±19%)	1.04(15) (±24%)	6.65(14) (±19%)
	Leakage (n/s)			
e. Leakage out of system per DT neutron	4.14(−3) (±10%)	4.28(−3) (±6%)	3.66(−3) (±8%)	3.22(−3) (±10%)

[a]In all cases, duct opening area = 0.567 m^2; bulk shield = 1.31-m-thick stainless-steel/B_4C alternate layers; penetration shield = 0.3-m-thick 50% stainless-steel + 50% B_4C around the duct; Monte Carlo (VIM) run with 20 000 neutron histories.
[b]The y direction is perpendicular to the midplane of the torus. The z direction is parallel to the toroidal magnetic axis.
[c]Normalized to a neutron wall loading of 1 MW/m^2.

Another possible incidental benefit is the reduction of the radiation streaming through the neutral beam ducts to the interior of the beam injectors because a fraction of the neutrons and photons escape into the evacuation side channels. Furthermore, this concept permits locating the vacuum pumping ducts at locations where the space problems of local exterior penetration shielding are less severe.

A sample of the results is shown in Table IX. Parameters for the reactor and duct system calculated are also shown in Table IX. The computations were carried out with the continuous energy Monte Carlo code VIM with 15 000 source neutron histories and nuclear data from ENDF/B-IV. The TF coils concentrically surround the bulk shield about the toroidal magnetic axis with an inner radius of 4.3 m, an outer radius of 4.9 m, and a width of 0.9 m in the present calculation. The side surface of the coils is away from the neutral beam duct center by 0.775 m. The position of the connected vacuum pumping duct axis (vertical to the midplane of the reactor) in case 2 is ~1.36 m from the end of the bulk shield and in case 3 is ~2.15 m. Although a relatively large size (0.75 m in diameter) for both the neutral beam duct and the vacuum pumping duct was chosen to reduce the statistical variance of the solution, the problem appears adequate enough to obtain a general insight into the effect of duct connection. The number in parenthesis in Table IX represents the statistical error as estimated by VIM.

It can be seen from the results in Table IX for location 1 that connecting the evacuation ducts to the beam ducts results in a very substantial reduction (a factor of ~30 in the present case) in the radiation level at the vacuum pumps. Obviously, the reduction has been brought about by blocking the direct streaming of neutrons into the connected vacuum pump system. This illustrates the significant benefits obtained by using a connected dual-purpose duct system. These results are also of great importance in that they clearly demonstrate that bends in ducts, if they are functionally allowed as in rf heating systems, serve to realize a better nuclear performance from a shielding point of view.

By comparing the two fluxes of cases 2 and 3 at location 2 in Table IX, we see that the duct connection away from the toroidal magnet region appears to slightly reduce the flux at the magnets (by ~7% increase with 0.2-m-thick shield in the present problem). From the results at locations 3 and 4 in Table IX, it is found that connecting the evacuation ducts to the neutral beam ducts does

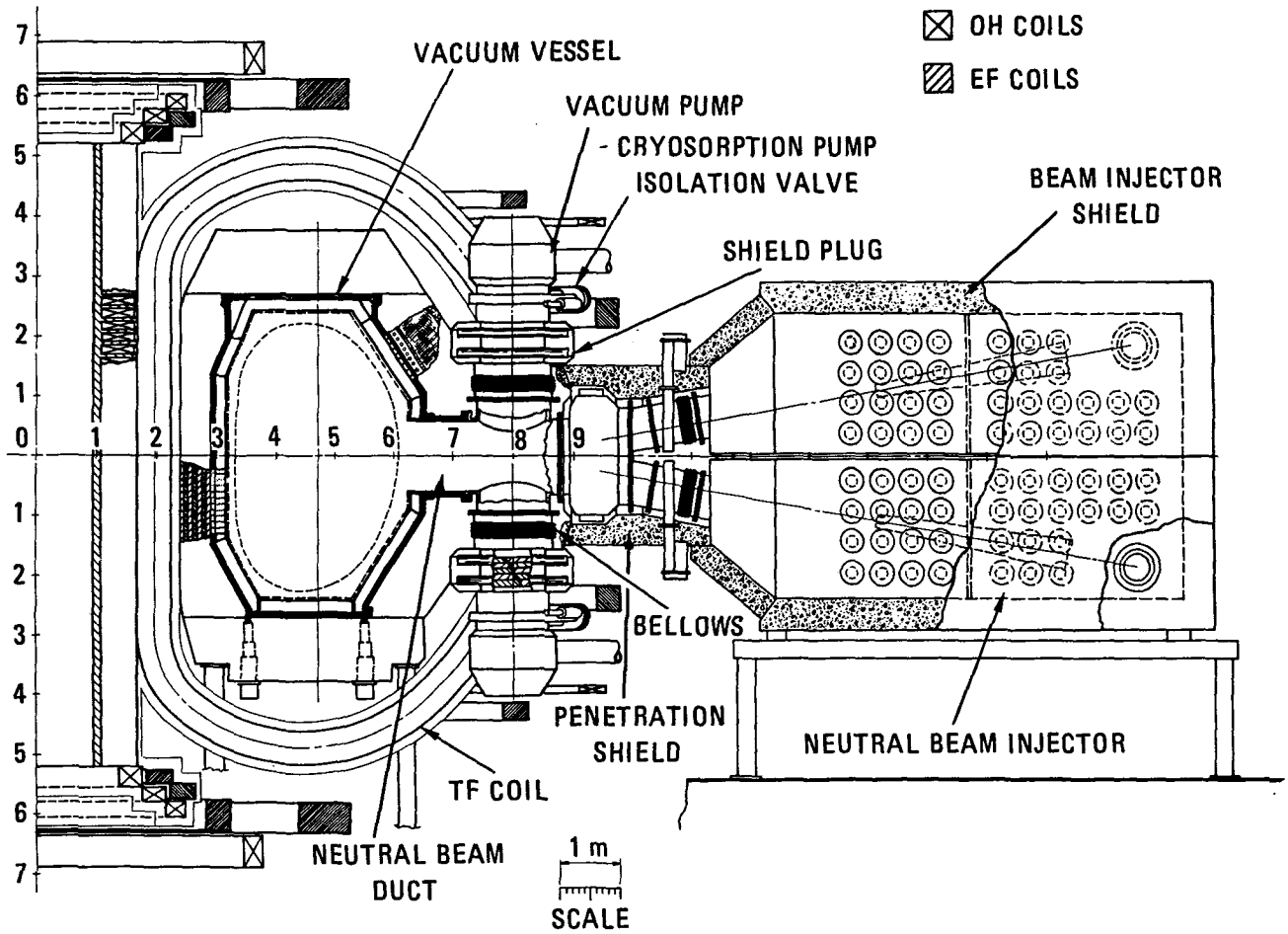

Fig. 8. A schematic vertical cross section of a tokamak with a dual-purpose duct for vacuum pumping and supplementary heating.

not significantly change the nuclear performance of the blanket/bulk shield regions in the vicinity of the beam ducts.

Branching off the particle stream into the evacuation side channels by duct connection seems to be small. Note that the results show somewhat unexpectedly that the neutron flux at the endcap of the neutral beam duct in case 3 is higher than that in cases 1 and 2. This may be attributable to the geometrical proximity of the endcap to the duct connection in case 3.

VI. rf HEATING SYSTEM

Supplementary plasma heating is a critical area of fusion reactor development. The two main approaches currently considered are (a) neutral beams and (b) rf. Assuming that the required technologies for both systems are available and that both can successfully heat the plasma, it is important to compare the two systems on the basis of performance and cost of the reactor. One such area of comparison is shielding. Neutral beam systems require straight-through ducts from the first wall to the beam injector chambers. The rf systems, on the other hand, tolerate various types of bends in their launching ducts.

Monte Carlo calculations were made using VIM for a lower hybrid rf system with a "grill" structure as shown in Fig. 9. We simplify the calculations somewhat by incorporating only the essential features of the system. The blanket is 0.3-m-thick stainless steel. Surrounding the blanket is a 0.6-m bulk shield of 50% stainless steel + 50% B_4C. A main duct with a 0.44- X 0.4-m rectangular aperture at the first wall is bent at right angles at ~0.9 m from the first wall upward and downward, and each branch has a rectangular cross section of 0.22 X 0.4 m. A second right-angle bend is made in each branch at a location elevated ~1 m from the centerline of the main duct, leading to the vacuum pumps. A 0.3-m-thick stainless-steel shield is provided to completely circumscribe all the rf ducts. In addition, a provision for 50% stainless-steel + 50% B_4C shield block is made for

TABLE IX

Effect of Connection of Vacuum Pumping Duct–Neutron Flux ($n/m^2 \cdot s$)

Location	Case 1[a]	Case 2[b]	Case 3[c]
1. Vacuum pump	7.56(-7) (±20%)	2.70(-8) (±15.3%)	2.35(-8) (±20.4%)
2. TF coils	4.25(-8) (±16.9%)	4.55(-8) (±11.7%)	3.27(-8) (±10.5%)
3. Neutral beam (NB) duct wall outside blanket/shield (2.2 m from first wall)	1.67(-6) (±19.1%)	---	1.36(-6) (±16.6%)
4. NB duct wall outside blanket/shield (3.0 m from first wall)	4.06(-7) (±12.8%)	4.63(-7) (±15.9%)	---
5. NB duct wall inside	2.37(-5) (±3.7%)	2.19(-5) (±4.8%)	2.18(-5) (±4.8%)
6. Endcap of NB duct	7.56(-7) (±20.4%)	6.79(-7) (±24.2%)	8.32(-7) (±20.8%)
7. System leakage	2.40(-3) (±11%)	2.37(-3) (±10%)	2.33(-3) (±14%)

Blanket/shield thickness	0.85 m (stainless-steel/B_4C layers)
Penetration shield thickness	0.20 m (50% stainless steel + 50% B_4C)
NB duct diameter	0.75 m
NB duct length	3.60 m
Vacuum duct diameter	0.75 m
Vacuum duct length	1.00 m
Normalization	1 source DT neutron
VIM Monte Carlo with 15 000 histories	

[a]No connection of evacuation duct.
[b]Evacuation duct connected to beam duct at a location 2.2 m away from first wall.
[c]Evacuation duct connected to beam duct at a location 3.0 m away from first wall.

region B in Fig. 9 to prevent radiation streaming into the reactor building. Table X shows the results of the calculations.

It is seen that if a dielectric window is placed in duct 2, the neutron dose accumulation averaged over the volume of duct 2 is $\sim 1.6 \times 10^{25}$ n/m^2 over a 1-yr reactor operation at a neutron wall loading of 1 MW/m^2. This neutron dose corresponds to an absorbed radiation dose of $\sim 7 \times 10^9$ Gy in the Al_2O_3 ceramic window. Therefore, radiation damage to insulators located in duct 2 is of concern. As shown in case 2 of Table X, removing the window to a location in waveguide 3 reduces the radiation level in the window by more than an order of magnitude compared to case 1. In particular, the neutron fraction with energy $E \geq 1$ MeV is almost negligible in case 2, and the fraction with $E \geq 0.12$ MeV is decreased from ~18% for case 1 to ~7% for case 2. An important observation to be made from the results in Table X is that the radiation level along the duct wall is much more rapidly attenuated in duct 3 (the ratio of the maximum-to-minimum flux is ~100) than in duct 1 where the ratio is only a factor of ~6. This is partly because the duct opening area of duct 3 is half of that of duct 1 and partly because the radiation streaming through the waveguides is significantly mitigated by the existence of the duct bends. It should be noted that the neutron flux of 4.7×10^{14} $(n/m^2 \cdot s)$ at the end of duct 3 (item 6 in Table X) is a factor of ~2 to 6 lower than that at the end of a typical neutral beam duct of ~5 m in length and ~0.5 m in diameter. These results demonstrate two particularly important points. First, the radiation streaming to the vacuum pumps of the rf system is much less than that to the pumping panels in the beam injector. The second important point is that radiation leakage to the reactor building is much higher with neutral beam systems than it is with rf systems. Protection of the equipment and control of the induced activation in the reactor building will require surrounding the huge chambers of the beam injectors with shielding; this represents an added cost item.

The neutron flux in region A in Fig. 9 is $\sim 9 \times 10^{17}$ $(n/m^2 \cdot s)$, which is just an order of magnitude below what one finds at the stainless-steel first wall for a neutron wall load of 1 MW/m^2. This implies that for rf systems one needs a shielding block in region B, as shown in Fig. 9, as well as the local shield surrounding the waveguides.

VII. NEUTRON SPECTRA

The extent to which radiation damage takes place by neutrons strongly depends on the energy spectra

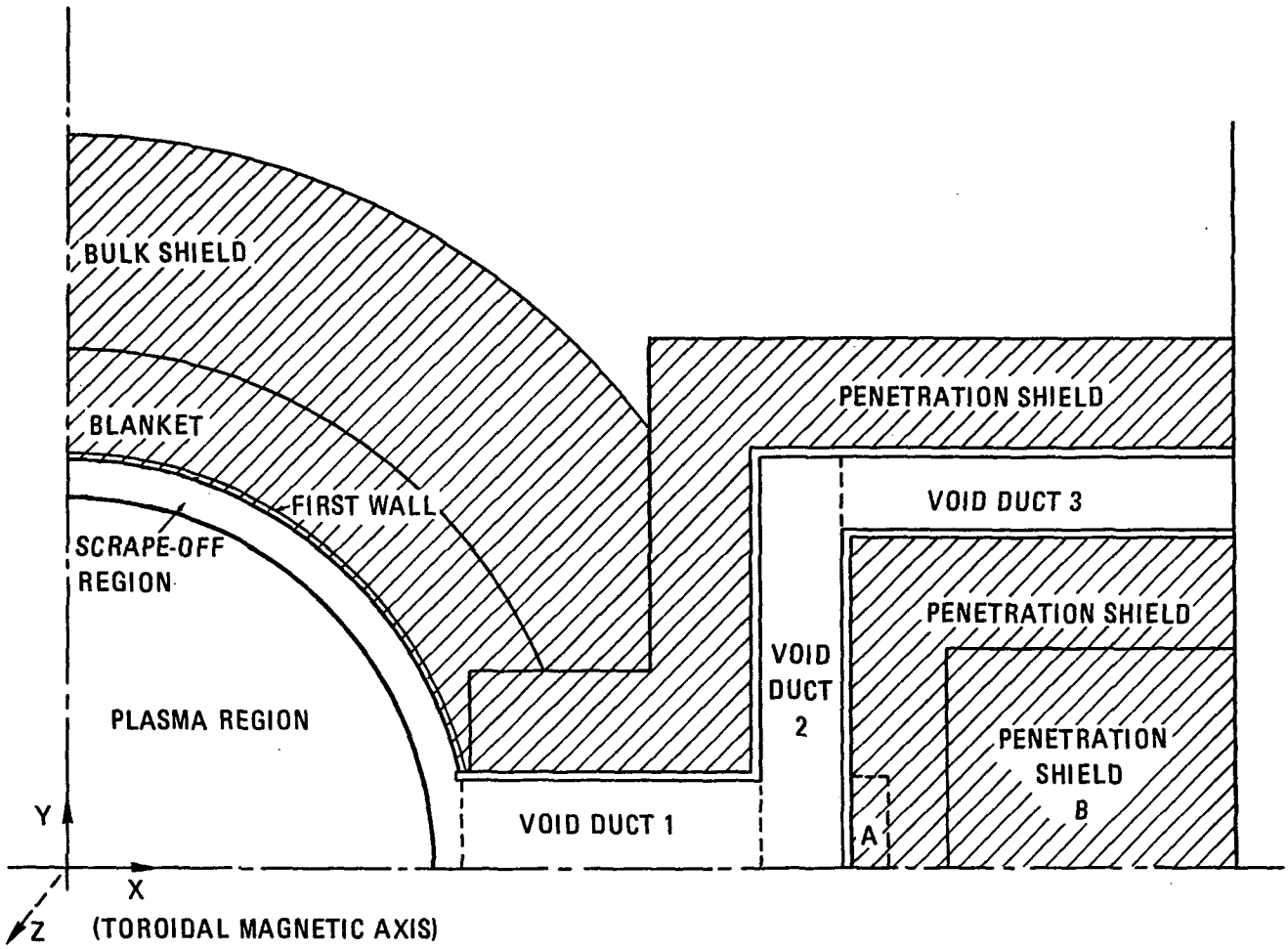

Fig. 9. A schematic diagram of a typical rf waveguide (ducts 1, 2, and 3) system.

of these particles. In this section, representative neutron spectra in the presence of fully shielded penetrations are examined. Calculations were made with a 0.5-m-thick local shield consisting of three concentric layers of stainless steel (0.05 m thick), 50% lead + 50% B_4C (0.35 m), and lead (0.10 m) for a duct having a 0.5-m diameter and a 5.5-m length. A 0.37-m-thick first wall/blanket region consisting of stainless steel is followed by a 0.25-m-thick coil coolant (20% H_2O + 10% stainless steel + 70% void) and a 0.25-m-thick normal copper coil. A provision is made for a double-layer bulk shield of 50% stainless steel + 50% B_4C and 50% stainless steel + 50% lead, which has an effective thickness of 0.75 m.

Figure 10 shows the neutron spectra along the stainless-steel duct wall. The spectrum at the TF coils is also shown for comparison. It is noted that the fluxes of the high-energy neutrons (>1 MeV) remain relatively high along the duct wall. Note also that the characteristic rise in the neutron flux per unit energy in the energy range from 10 to 14 MeV is persistent. The spectrum at the point that is close to the beam injector entrance (5 m away from the first wall) is two to three orders of magnitude higher than that at the TF coils. This implies that the reactor activation problem is more serious in the structure of the beam chamber rather than in the TF coils. This observation is particularly important in design efforts aimed at reducing the biological dose in the reactor building after shutdown.

Figure 11 shows the fraction $f(E_0)$, of the total neutron flux with neutron energies above E_0 as a function of E_0 for the same locations as those in Fig. 10. At the first wall, the fraction $f(E_0 > 10$ MeV) is ~10%, mostly coming from the DT source neutrons that have not collided. The fraction with energy $E_0 > 1$ MeV reaches ~25% at the first wall, compared to a nearly constant value of ~10% along the duct, as evident from Fig. 11. At the TF coils, the fraction of the neutrons with energies above 4 MeV is small (~1%). The fraction of neutrons with energies >1 MeV at the TF coils is less than that along the duct wall because many neutrons are slowed down and absorbed in the thick penetration shield before they reach the toroidal magnet regions.

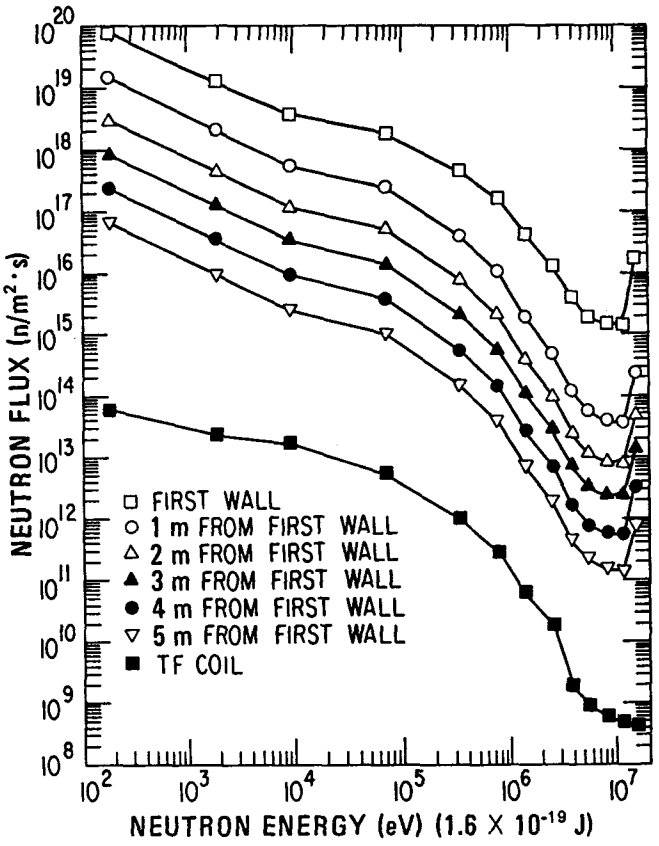

Fig. 10. Neutron spectra along the duct wall and at the TF coils for a neutron wall loading of 0.1 MW/m².

ACKNOWLEDGMENT

This work was supported by the U.S. Department of Energy.

REFERENCES

1. M. A. ABDOU, L. MILTON, J. JUNG, and E. M. GELBARD, "Multidimensional Neutronics Analysis of Major Penetrations in Tokamaks," *Proc. 2nd ANS Topl. Mtg. Technology of Controlled Nuclear Fusion*, CONF-760935-P3, p. 845, U.S. Energy Research and Development Administration (1976).

2. M. A. ABDOU and J. JUNG, "Nuclear Analysis of a Tokamak Experimental Power Reactor Conceptual Design," *Nucl. Technol.*, 35, 51 (1977).

3. T. IDE, Y. SEKI, and H. IIDA, "Effects of Neutron Streaming Through Injection Ports on Neutronic Characteristics of a Fusion Reactor," *Proc. 2nd ANS Topl. Mtg. Technology of Controlled Nuclear Fusion*, CONF-760935-P2, p. 395, U.S. Energy Research and Development Administration (1976).

4. R. T. SANTORO et al., "Monte Carlo Analysis of the Effects of a Blanket-Shield Penetration on the Performance of a Tokamak Fusion Reactor," ORNL/TM-5874, Oak Ridge National Laboratory (1977).

TABLE X

Lower Hybrid rf System Shielding Analysis

A. Neutron fluence[a] at dielectric window (n/m²·yr)	
1. in duct 2	1.57[a](25) (±7%)[b]
2. in duct 3	9.34(23) (±27%)
B. Neutron flux[a] (n/m⁻²·s⁻¹)	
in the walls of duct 1:	
3. maximum	4.69(18) (±2%)
4. minimum	7.82(17) (±10%)
in the walls of duct 3	
5. maximum	4.86(16) (±24%)
6. minimum	4.67(14) (±40%)
7. at location A in Fig. 9	9.06(17) (±6%)
C. Neutron leakage per DT neutron	3.16(−4) (±33%)

Duct 1–0.8 m (x)[c] X 0.44 m (y)[d] X 0.4 m (z)[e]
Duct 2–0.22 m (x) X 1.11 m (y) X 0.4 m (z)
Duct 3–1 m (x) X 0.22 m (y) X 0.4 m (z)

Blanket	0.3-m-thick stainless steel
Bulk shield	0.6-m-thick (50% stainless steel + 50% B_4C
Penetration shield	0.3-m-thick stainless steel all around the waveguides.

[a]Normalized to a neutron wall loading of 1 MW/m².
[b]Monte Carlo calculation run with 15 000 neutron histories.
[c]The x direction is perpendicular to the toroidal magnetic axis.
[d]The y direction is perpendicular to the midplane of the torus.
[e]The z direction is parallel to the toroidal magnetic axis.

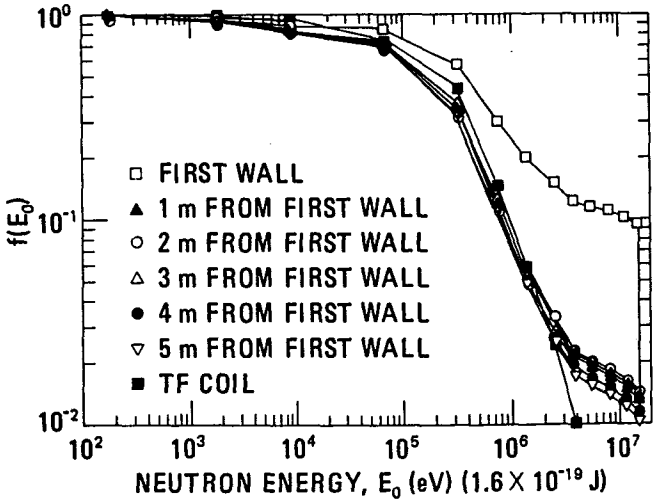

Fig. 11. Fraction, $f(E_0)$, of neutrons with energy larger than E_0 along the duct wall and at the TF coils.

5. Y. GOHAR and C. W. MAYNARD, "Tokamak Divertor Slot Design to Enhance Magnet Shielding," *Trans. Am. Nucl. Soc.*, **26**, 508 (1977).

6. E. M. GELBARD and R. E. PRAEL, "Monte Carlo Work at Argonne National Laboratory," *Proc. NEACRP Mtg. Monte Carlo Study Group*, ANL-75-2 (NEA-CRP-L-118), p. 201, Argonne National Laboratory (1975).

7. R. E. PRAEL and L. J. MILTON, "A User's Manual for the Monte Carlo Code VIM," FRA-TM-84, Argonne National Laboratory Internal Memorandum (1976).

8. O. OZER and D. GARBER, "ENDF/B Summary Documentation," BNL-17541 and ENDF-201, Brookhaven National Laboratory (1973).

9. D. GARBER, Compiler, "ENDF/B Summary Documentation," BNL-17541, Brookhaven National Laboratory (1975).

10. D. M. PLASTER, R. T. SANTORO, and W. E. FORD III, "Coupled 100-Group Neutron and 21-Group Gamma-Ray Cross Sections for EPR Calculations," ORNL-TM-4872, Oak Ridge National Laboratory (1975).

11. N. M. GREENE et al., "AMPX: A Modular Code System for Generating Coupled Multigroup Neutron-Gamma Libraries from ENDF/B," ORNL/TM-3706, Oak Ridge National Laboratory (1976).

12. "GAS-ANL TNS Scoping Studies, Vol. I, Summary," GA-A14614-Vol. I, General Atomic Company (1977).

13. M. A. ABDOU, "Radiation Considerations for Superconducting Fusion Magnets," ANL/FPP/TM-92, Argonne National Laboratory Internal Memorandum (1977); also, B. S. BROWN, T. H. BLEWITT, T. L. SCOTT, and A. C. KLARK, "Low-Temperature Fast-Neutron Radiation Damage Studies in Superconducting Materials," *J. Nucl. Mater.*, **52**, 215 (1974); also, B. S. BROWN, "Radiation Effects on Superconductivity," in *Radiation Damage in Metals*, N. L. PETERSON and S. D. HARKNESS, Eds., American Society for Metals (1975).

14. C. A. M. VAN DER KLEIN, "The Organic Insulator in Fusion Reactor Magnet Systems," RCN-240, Reactor Centrum Nederland (1975).

15. F. W. CLINARD, Jr., J. M. BUNCH, and W. R. RANKEN, "Neutron Irradiated Damage in Al_2O_3 and Y_2O_3," in *Radiation Effects and Tritium Technology for Fusion Reactors*, CONF-750989, Vol. II, p. 498, U.S. Atomic Energy Commission (1975).

16. W. M. STACEY, Jr. et al., "Tokamak Experimental Power Reactor," *Proc. IAEA Workshop Fusion Reactor Design*, Madison, Wisconsin, October 10-21, 1977; also, *Nucl. Fusion* (to be issued).